TITLE: INSIDE-OUT REGULATION OF E-CADHERIN CONFORMATION AND ADHESION

AUTHORS: Ramesh Koirala[1,2,#], Andrew Vae Priest[1,2,#], Chi-Fu Yen[2], Joleen S. Cheah[1], Martijn Gloerich[3], Soichiro Yamada[1], Sanjeevi Sivasankar[1*]

AFFILIATIONS: [1]Department of Biomedical Engineering, University of California, Davis, CA 95616; [2]Department of Physics and Astronomy, Iowa State University, Ames, IA 50011; [3]Molecular Cancer Research, Center for Molecular Medicine, University Medical Center Utrecht, Utrecht, The Netherlands.

[#] Equal contribution

* Corresponding author: ssivasankar@ucdavis.edu

ABSTRACT: Cadherin cell-cell adhesion proteins play key roles in tissue morphogenesis and wound healing. Cadherin ectodomains bind in two conformations, X-dimers and strand-swap dimers, with different adhesive properties. However, the mechanisms by which cells regulate ectodomain conformation are unknown. Cadherin intracellular regions associate with several actin-binding proteins including vinculin, which are believed to tune cell-cell adhesion, solely by remodeling the actin cytoskeleton. Here, we demonstrate that vinculin association with the cadherin cytoplasmic region, also allosterically regulates ectodomain structure and adhesion, by converting weaker X-dimers into stronger strand-swap dimers. We also show that in epithelial cells, only half of apical cadherins are linked to the cytoskeleton. Furthermore, only 70% of apical cadherins form strand-swap dimers while the remaining form X-dimers, which provides cells with two cadherin pools with different adhesive properties. Our results showing allosteric modulation of adhesion at the single-molecule level are the first demonstration of inside-out regulation of cadherin conformation.

INTRODUCTION

E-cadherins (Ecads) are essential, calcium dependent cell-cell adhesion proteins that play key roles in the formation of epithelial tissue and in the maintenance of tissue integrity. Ecad adhesion is highly plastic and carefully regulated to orchestrate complex movement of epithelial cells and dysregulation of adhesion is a hallmark of numerous cancers [1]. However, little is known about how cells dynamically regulate the biophysical properties of individual Ecads.

The extracellular regions of Ecads from opposing cells bind in two distinct *trans* orientations: strand-swap dimers and X-dimers. Strand-swap dimers are the stronger cadherin adhesive conformation and are formed by the exchange of conserved Tryptophan (Trp) residues between the outermost domains of opposing Ecad [2, 3, 4]. In contrast, X-dimers, which are formed by extensive surface interactions between opposing Ecad, are a weaker adhesive structure and serve as an intermediate during the formation and rupture of strand swap dimers [5, 6, 7]. Using cell-free, single molecule experiments, we previously showed that X-dimers and strand-swap dimers can be distinguished based on their distinctly different response to mechanical force. When a strand-swap dimer is pulled, its lifetime decreases with increasing force, resulting in the formation of a slip bond [8, 9]. In contrast, an X-dimer responds to pulling force by forming a catch bond, where bond lifetime initially increases up to a threshold force, and then subsequently decreases [8, 10]. We also showed that wild type Ecad ectodomains in solution can interconvert between X-dimer and strand-swap dimer conformations [9]. However, the biophysical mechanisms by which Ecad conformations (and adhesion) are regulated on the cell surface are unknown.

The cytoplasmic region of Ecad associates with p120-catenin and β-catenin and recruits the actin binding and bundling protein α-catenin. The Ecad-catenin complex links to filamentous actin (F-actin) either by the direct binding of α-catenin and F-actin or by the indirect association of α-catenin and F-actin via vinculin [11] (Figure 1A). Adhesive forces transmitted across intercellular junctions by Ecad induce conformational changes in α-catenin [12, 13], strengthen F-actin binding [14] and recruit vinculin to the sites of force application [15, 16]. However, vinculin and α-catenin do not merely serve as passive cytoskeletal linkers; they also dynamically modulate cytoskeletal rearrangement and recruit myosin to cell-cell junctions [12, 17, 18, 19]. Studies show that α-catenin and vinculin play important roles in strengthening and stabilizing Ecad adhesion: bead twisting experiments show force-induced stiffening of Ecad-based junctions and cell doublet stretching experiments demonstrate reinforcement of cell-cell adhesion in vinculin and α-catenin dependent manners [17, 19, 20]. Consequently, actin anchorage and cytoskeletal remodeling are assumed to be the exclusive mechanisms by which α-catenin and vinculin strengthen Ecad adhesion [21, 22, 23]. Here, we directly map the allosteric effects of cytoplasmic proteins and demonstrate, at the single molecule level, that vinculin association with the Ecad cytoplasmic region switches X-dimers to strand-swap dimers, thereby regulating ectodomain structure and adhesion.

RESULTS

Single molecule Atomic Force Microscope (AFM) measurements of specific Ecad *trans* adhesion. We measured interactions between recombinant Ecad extracellular regions immobilized on AFM cantilevers and Ecad endogenously expressed on the apical

surface of confluent Madin-Darby Canine Kidney (MDCK) cell monolayers (Figure 1B). To ensure that we measured single Ecad unbinding events, we immobilized Ecad on the AFM tip at low density and pressed on the cell surface with a low initial contact force (mean pressing force = 56 pN; Figure S1). Poisson statistics predict that even the maximum event rate we measure (18%; Figure 2A) corresponds to 90% probability of measuring single molecule events.

Our experiments were performed with the following MDCK cells: parental cells (*parental*), vinculin knockout cells (*vinc-KO*), α-catenin knockout cells (*αcat-KO*) [24], αcat-KO cells rescued with α-catenin lacking the vinculin binding site (*ΔVBS*) [25], and Ecad knockout cells (*Ecad-KO*) (Figure 1C). We also performed measurements with parental cells in the presence of free tryptophan (*parental-Trp*) in order to trap Ecad in an X-dimer conformation [8]. We quantified the specific and nonspecific binding rates for every cell line by measuring the event rate of single unbinding events using either AFM tips that were decorated with Ecad (specific binding) or AFM tips that lacked Ecad (nonspecific binding). In the parental, parental-Trp, αcat-KO, vinc-KO, and ΔVBS cells, we observed a significant increase in single unbinding events when the AFM tips were decorated with Ecad (Figure 2A). In contrast, in the Ecad-KO cells, event rates using AFM tips with/without Ecad were similar to each other and were comparable to the nonspecific event rates measured with the other cell lines (Figure 2A). Taken together, this confirmed that the measured specific events corresponded to Ecad-Ecad binding interactions.

Ecad conformation and cytoskeletal-linkage in each cell line were determined from previously reported 'signatures' in the measured force curves. Since force measurements have shown that pulling on a cell surface protein that is not linked to the cytoskeleton results in the formation of a *membrane-tether* [26, 27] (Figure 3A), we used membrane-tethers

to identify Ecad that are uncoupled from the actin cytoskeleton (Figure 3B). Previous studies have also shown that pulling on a transmembrane protein that is firmly bound to the underlying cytoskeleton results in a linearly elastic response to pulling force [28, 29] (Figure 3C). Since these *jump* events occur when interactions between proteins on the AFM tip and cell surface are weaker than the protein-cytoskeleton linkage, we interpreted jumps as a signature of actin-linked Ecad proteins that form weak *trans* dimers, which rupture before failure of the Ecad-cytoskeletal linkage (Figure 3D). Finally, if the Ecad *trans* dimers adhere robustly compared to the Ecad-cytoskeletal linkage, an initial steep increase in force is measured which relaxes viscoelastically when the Ecad-cytoskeletal bond ruptures, resulting in the formation of a *cyto-tether* (Figure 3E-F). To further validate tether formation , we fit the membrane-tether and cyto-tether force-extension curves to the standard linear solid (SLS) model (SI Note 1) [30]. The SLS fitting parameters we obtained for the tethers, were consistent with previous values obtained for tether formation on Jurkat cells and T-cells (Table S1) [30, 31].

About 50% of non-junctional Ecads are coupled to the actin cytoskeleton. We first compared the fraction of Ecad uncoupled from the cytoskeleton (membrane-tethers) to the fraction of Ecads that are coupled to cortical actin (cyto-tethers and jumps). Our data showed that in parental cells, 52% ± 9% of Ecad on the apical surface of the cell are uncoupled from the actin cytoskeleton (Figure 2B). Since α-catenin is believed to be vital in mediating Ecad linkage to F-actin, we next measured the cytoskeletal linkage of Ecad in αcat-KO cells. As anticipated from previous biochemical and cell biological results [32, 33], our data showed that the vast majority of Ecad (91% ± 13%) in αcat-KO cells are uncoupled from the actin cytoskeleton (Figure 2B). In contrast, the fraction of uncoupled

Ecads in both vinc-KO and ΔVBS cells, where Ecads are presumably weakly linked to F-actin by α-catenin, but where this linkage is not reinforced by vinculin [12, 34], was comparable to parental cells (65% ± 9% for vinc-KO and 48% ± 4% for ΔVBS cells; Figure 2B). Taken together, this data confirms the obligatory role of α-catenin in mediating Ecad linkage to F-actin. These direct, single molecule measurements of Ecad-actin coupling on the apical surface of live cells are in excellent agreement with previous single particle tracking of Ecad on the cell surface that inferred approximately 50% of Ecads on the apical surface of cells are coupled to the actin cytoskeleton [35].

Ecad ectodomain conformation is regulated by vinculin. Next, we proceeded to identify the binding conformation of Ecad ectodomains in the different cell lines by measuring if the Ecads on the cell surface form catch bonds (X-dimers) or slip bonds (strand-swap dimers). We measured the force *vs.* lifetimes of Ecad-Ecad bonds, using a method described previously [36]. Briefly, since the force required to rupture membrane-tethers and cyto-tethers scales linearly with pulling velocity [27, 37] (Figure S2), and because these tethers extend at a constant force (after any initial viscoelastic relaxation) when pulled at a constant velocity [26, 30] (Figure 3A, 3E), we determined bond lifetimes at a range of forces from the persistence time of membrane-tethers and cyto-tethers.

We first measured the force *vs.* lifetime of Ecad endogenously expressed on the apical surface of parental cells. Fits of our data to the composite of a slip bond [38] and catch bond [39] model showed that 73% of Ecad in the parental cells form strand-swap dimers while the remaining 27% of Ecad occupy an X-dimer conformation (Figure 4A; Methods; Table S2). Since we have previously shown, using cell-free experiments, that Ecad

ectodomains can be trapped in an X-dimer conformation, simply by incubating them in free Trp [8], we proceeded to incubate the parental cells with Trp and measure the force-dependent lifetimes of Ecad-Ecad bonds. Our measurements showed that upon Trp incubation, Ecads in parental cells switched their conformation and formed catch bonds characteristic of an X-dimer (Figure 4B). Importantly, switching ectodomains into an X-dimer conformation did not decouple Ecad from the cytoskeleton; the fraction of cytoskeleton-coupled Ecad in the Trp treated cells (53% ± 5%) remained the same as parental cells (Figure 2B).

Since the bond-lifetimes for parental cells (Figure 4A) were obtained from all the tethers (a mix of cyto-tethers and membrane-tethers), we separately analyzed the force-dependent lifetimes of cyto-tether and membrane-tether events (Figure S3). Our analysis showed that while cyto-tethers (which correspond to Ecad initially coupled to the cytoskeleton) exclusively formed slip-bonds, Ecad that were decoupled from the cytoskeleton (membrane-tether events) formed X-dimers and strand-swap dimers with almost equal probabilities (54% catch bonds: 46% slip bonds) (Figure S3). This suggested to us that the association of α-catenin and/or vinculin with the Ecad cytoplasmic domain, may be required for ectodomains to efficiently form strand-swap dimers.

In striking agreement, in the vinc-KO cells, the Ecads formed catch bonds characteristic of an X-dimer conformation (Figure 4C) suggesting that vinculin association is necessary for Ecads to form robust strand-swap dimers. Similarly, Ecads in αcat-KO cells, where vinculin cannot associate with the Ecad cytoplasmic region [11], also formed catch bonds (Figure 4D). Finally, eliminating vinculin binding to α-catenin in ΔVBS cells also resulted in catch bonds (Figure 4E), confirming that association of vinculin with the

Ecad cytoplasmic region via α-catenin is obligatory for transitioning from a weak X-dimer conformation to a robust strand-swap dimer conformation.

In absence of vinculin, cytoskeleton-coupled Ecad also form X-dimers. Having determined Ecad conformation from the lifetimes of membrane-tethers and cyto-tethers, we next compared the fraction of weak (jumps) and strong (cyto-tethers) *trans* dimers, formed by cytoskeleton-coupled Ecad. Our data showed that in parental cells that contain both α-catenin and vinculin, 85% ± 9% of cytoskeleton-coupled Ecad bind robustly while the remaining 15% ± 8% of Ecad interact weakly (Figure 4F). In contrast, in vinc-KO cells, only 8% ± 9% of cytoskeleton-coupled Ecad bind in a robust binding conformation (Figure 4F). Similarly, in ΔVBS cells where vinculin cannot bind to α-catenin, only 3% ± 4% of cytoskeleton-linked Ecad bind in a robust binding conformation (Figure 4F). Taken together, this indicates that vinculin association with the Ecad cytoplasmic region is required for robust Ecad *trans* dimerization which is in agreement with our force *vs.* lifetime measurements. Strikingly, when parental cells were incubated with Trp, almost all (98% ± 5%) cytoskeleton-bound Ecads formed weak *trans* dimers (Figure 4F) confirming that the jump events correspond to the X-dimer structures. It is important to point out that the strength of *trans* dimer adhesion in the absence of α-catenin could not be determined by comparing the fraction of cyto-tethers and jumps because jump events were extremely rare in the αcat-KO cells.

We also inferred the *trans* dimer binding conformation of cytoskeleton-coupled Ecad in the parental-Trp, vinc-KO and ΔVBS cells using dynamic force spectroscopy analysis [40]. The measured k_{off} for jump events for vinc-KO and ΔVBS (k_{off} = 2.19 ± 1.26 s^{-}

[1]; Figure S4A) was comparable to parental-Trp X-dimers (k_{off} =1.41 ± 0.75 s^{-1}; Figure S4B), and higher than previously published values for strand-swap dimers [41, 42, 43, 44]. Since a higher k_{off} corresponds to a weaker binding, this data confirms that in the absence of vinculin association, Ecads adopts a weaker X-dimer conformation.

DISCUSSION

Using live-cell, single molecule AFM measurements, we directly demonstrate inside-out regulation of cadherin conformation and show that cytoplasmic proteins regulate Ecad adhesive properties, similar to inside-out regulation of integrins [45]. While previous AFM measurements with α-catenin knockdown cells suggest that reducing α-catenin levels decrease the unbinding force of Ecad ectodomains, the molecular mechanism by which α-catenin influences Ecad adhesion was not determined [46, 47]. Our data shows that vinculin association triggers the allosteric strand-swap dimerization of Ecad, while α-catenin affects Ecad adhesion by serving as the scaffold protein that binds vinculin to Ecad-catenin complex.

Our results also demonstrate that previous interpretations of how vinculin strengthens Ecad adhesion are incomplete. While these studies solely focused on vinculin mediated remodeling of intercellular junctions [21, 22, 23], we demonstrate that vinculin also changes the adhesive properties of individual Ecad ectodomains. Although the allosteric mechanism by which vinculin regulates Ecad conformation is unclear, it is possible that mechanical force exerted by cytoskeletal contractility transmits through vinculin to the Ecad ectodomain and drives the conversion of X-dimers to strand-swap dimers. Consequently, when Ecads decouple from vinculin, they are trapped in an X-dimer

structure. Additionally, association of vinculin with the Ecad cytoplasmic region may lock Ecad in an orientation that allows the exchange of partner amino acids required for strand-swap dimerization.

While Ecad that are coupled to the cytoskeleton via α-catenin and vinculin (cyto-tethers) exclusively formed strand-swap dimers, we were surprised to observe that Ecad that are decoupled from the cytoskeleton (membrane-tethers) formed X-dimers and strand-swap dimers with coequal probabilities (Figure S3). A likely explanation for this result is that the Ecad-cytoskeletal linkage is dynamic and that even transient interactions with vinculin are sufficient to drive strand-swap dimer formation. Since the AFM-tip and the cell surface remain in contact for about 0.4s in our experiments (Figure S5), this may allow enough time from Ecads on the parental cells to convert to a strand-swap dimer conformation and detach from the cytoskeleton (thereby forming membrane-tethers), before the AFM-tip is withdrawn from the cell surface.

Consistent with a previous study that used optical tweezers and single particle tracking to infer the fraction of cytoskeleton-bound Ecad [35], our data shows that only ~50% of Ecads on the apical cell surface are coupled to the actin cytoskeleton. Studies also show that cells expressing Ecad/α-catenin fusion constructs that constitutively bind to the actin cytoskeleton, exhibit higher cell-cell adhesion and reduced intercellular motility compared to cells expressing wild type Ecad [35, 48]. These findings are supported by our observation that while Ecads that are robustly coupled to actin form strand-swap dimers, Ecads that are decoupled from the cytoskeleton can form either X-dimers or strand-swap dimers, suggesting that two rapidly exchangeable pools of Ecad structures exist on the cell surface. It is likely that these different pools of Ecads are crucial in reorganizing cell-cell junctions during collective cell migration: as the cell-cell contacts rapidly rearrange,

strand-swap dimers anchor the contact while X-dimers probe for formation of new contacts.

Despite the large number of proteins expressed on the cell surface, we were still able to measure single-molecule unbinding by limiting Ecad density on the AFM tip and controlling the force with which the AFM tip contacts the cell. However, we were also aided by a low density of Ecads expressed on the apical surface of confluent MDCK cell monolayers. While the precise oligomeric state of Ecad on apical cell surfaces is unclear, with super-resolution imaging suggesting that apical Ecads in A431 cells are present as well separated monomers [49] while Ecads in A431D cells organize into small nanoclusters [50], our low unbinding event rates nonetheless suggest that only single Ecad on the AFM tip interact with Ecad on the cell surface. Interestingly, the total Ecad event rate measured with αcat-KO cells is higher than with parental, ΔVBS or vinc-KO cells (Figure 2A). This likely occurs because the αcat-KO cells do not form stable cell-cell junctions [24]. Consequently, Ecads that would otherwise be corralled within cell-cell junctions are now redistributed on the apical cells surface and subsequently interact with Ecads on the AFM tip with a higher probability. The same may be true for other membrane proteins which contributes to an increase in non-specific event rate in control experiments with αcat-KO cells (Figure 2A).

Previous studies suggest that Ecad adhesion is altered by changing the phosphorylation state of cytoplasmic p120-catenin [43, 51, 52]; however, the mechanism by which this occurs and exact conformational states Ecads adopt, are unknown. It is possible that p120-catenin also modulates vinculin association with the Ecad cytoplasmic region, which in turn regulates Ecad ectodomain conformation and adhesion. Finally, recent studies have suggested that regulation of Ecad adhesion plays an important role in

cancer progression. For instance, it has been shown that up-regulation of Ecad adhesive activity, rather than its amount, reduces the number of cells metastasized from the mammary gland to the lung [53]. Additionally, several point mutations in Ecad ectodomains that are prevalent in hereditary diffuse gastric carcinoma selectively interfere with the inside-out regulation of Ecad adhesion, rather than the ability of Ecad to adhere [53]. Furthermore, studies have shown that while vinculin expression is significantly reduced in colorectal cancer (CRC), overexpressing vinculin reduces metastasis in CRC [54] and other cancer cell lines [55]. Consequently, understanding how cytoplasmic proteins induce conformational changes of Ecad ectodomains could be crucial to understanding the role of Ecad in cancer progression and metastasis.

METHODS

Purification of Ecad ectodomain. Generation of Ecad monomer plasmids containing a C-terminal Avi tag has been described previously [56]. The plasmids were incorporated into pcDNA3.1(+) vectors and were transiently transfected into HEK 293T cells using PEI (Milipore Sigma) as previously described [57]. Three days post transfection, conditioned media was collected for protein purification. Purification of Ecad were performed using methods described previously [8, 56]. Media containing his-tagged Ecads was passed through a chromatography column containing Ni-NTA agarose beads (Qiagen). Beads were then washed with a pH 7.5 biotinylation buffer (25mM HEPES, 5mM NaCl, and 1mM $CaCl_2$). Ecads bound to the Ni-NTA beads were biotinylated with BirA enzyme (BirA 500 kit; Avidity) for 1hr at 30^0C. Following biotinylation, free biotins were removed using the

Ni-NTA column and biotinylated Ecads bound to Ni-NTA beads were eluted using a pH 7.5 buffer containing 200mM Imidazole, 20mM Na_2HPO_4, 500mM NaCl, and 1mM $CaCl_2$.

Ecad functionalization on AFM cantilever. Purified Ecad monomers were immobilized on Si tip of AFM cantilevers (Hydra 2R-100N; AppNano) as described previously [8, 9, 56, 58]. Briefly, the AFM cantilevers were cleaned by immersing in 25% H_2O_2/ 75% H_2SO_4 solution overnight. The cantilevers were then sequentially washed with deionized water and acetone. The cantilevers were functionalized with amine groups by immersing in 2% (vol/vol) 3-aminopropyltriethoxysilane (Millipore Sigma) solution dissolved in acetone. Polyethylene glycol (PEG) (MW 5000, Lysan Bio) spacers containing amine-reactive N-hydroxysuccinimide ester group at one end were covalently attached to the cantilever (100 mg/ml in 100mM $NaHCO_3$ dissolved in 600mM K_2SO_4, for 4 hrs); 20% of the PEG spacers presented biotin molecules at the other end. Unreacted amine groups on the silane molecules were capped using NHS-sulfo acetate (10 mg/ml for 30 mins; Thermo Fisher). PEG-functionalized AFM cantilevers were incubated in 1 mg/ml Bovine Serum Albumin [58] overnight. The cantilevers were then sequentially incubated with streptavidin (0.1 mg/ml for 30 mins) and biotinylated Ecads (200 nM for 90 mins). Finally, free biotin-binding sites of streptavidin were blocked by using 0.02 mg/ml free biotin for 20 mins. All steps, except the incubation with Ecad, were kept the same for cantilever functionalization in control experiments.

Cell culture for AFM experiment. Cells were cultured in low glucose Dulbecco's modified Eagle's medium (DMEM) (Milipore Sigma) supplemented with 10% FBS (Milipore Sigma)

and 1% antibiotics solution (penicillin + streptomycin + kanamycin) at 37^0C and 5% CO_2. Cells were trypsinized 48-72 hrs prior to the experiment and plated on an ethanol-cleaned glass coverslip at a low density. The confluent monolayer of cells was washed 5 times with a pH 7 DMEM and antibiotics solution before loading onto the AFM setup with the same medium.

AFM force measurements. Force measurements were performed using two Agilent 5500 AFMs with closed loop scanners. An AFM cantilever functionalized with purified Ecad was brought in contact with a confluent monolayer of cells, pressed against the cell surface with a low force (typical pressing force was about 50 pN) for 0.1s, and then retracted at one of five constant velocities (3, 5, 7, 9, 11 µm/s). Control experiments used cantilevers decorated with streptavidin but lacking Ecad. Cantilever spring constants were measured using the thermal fluctuation method [59]. All the experiments were performed in a pH 7 DMEM and antibiotics solution in a custom-built environmental chamber supplied with 5% CO_2. Parental-Trp experiment was performed with 2mM L-Tryptophan (Alfa Aesar) in the solution. A typical experiment lasted for ~10 hours yielding ~1200 force-distance traces.

Generating mutant cell lines. Generation of αcat-KO cells (ΔαE-catenin MDCK cells) [24] has been described previously. For generation of ΔVBS cells, αcat-KO cells were stably rescued [25] with GFP-α-catenin–ΔVBS mutants [34] as described previously. Vinc-KO and Ecad-KO cells were generated by stably expressing a PiggyBac plasmid encoding Cas9 with a cumate inducible promoter, and gRNA expression cassette for canine Ecad or vinculin specific gRNA, which resulted in complete knockout cells (see Figure 1C). The

mutations were sequence verified by PCR amplifying the target sequences from genomic DNA of knockout cell lines and inserted into TOPO vectors (Invitrogen) for sequencing.

Ecad:

gRNA: ACAGACCAGTAACTAACGA

KO: ACAGACCAGT----AACGA

Vinculin:

gRNA: GGA GCACCGAGTAATGTTGG

KO: GGAtGCACCGAGTgATGTTGG

Analysis of AFM data. AFM-generated force-distance traces were analyzed using custom MATLAB scripts. Traces containing single rupture events were classified into membrane-tether, jump, and cyto-tether categories based on the following criteria:

- Membrane-tethers: force plateau at least 100nm long and slope less than 25 pN/μm.
- Cyto-tethers: have a difference of at least 5 pN between the peak force and the plateau force.
- Jumps: have a linear force-distance relationship with a slope of more than 25 pN/μm.

Rupture events having unbinding force <5 pN were not considered for analysis. Tethers were further fit to the SLS model as described in [30] while jumps were fit to a Hookean spring model. We only retained events that fit either the SLS or spring model

with a Root Mean Squared Error (RMSE) of less than the mean plus two standard deviations of all fits for each respective model.

To obtain the fractions of membrane-tether, cyto-tether, and jump events for each cell line, we first measured the binding probability of each type of event for both the Ecad experiment and the control. The binding probabilities obtained from the control experiment were subtracted from the corresponding event rate of the Ecad experiment.

Loading rates for the jump events used for dynamic force spectroscopy analysis (Figure S4) were calculated by multiplying the slope of the jump by the pulling velocity. K-means clustering was used to group the loading rates as described previously [60]. Mean unbinding force and mean loading rate for the groups were fit using non-linear least square fit to the Bell-Evans model [40]. To estimate the errors in fitting parameters, raw data was bootstrapped with replacement, grouped using k-means, and the mean values were fit to the Bell-Evans model 1000 times; the standard deviations of the resulting distributions of parameters was then calculated.

Force-dependent Ecad-Ecad bond mechanics were studied by analyzing the forces and lifetimes of membrane-tethers and cyto-tethers. Bond lifetimes were determined from the force curves starting at the beginning of the plateau region to the bond rupture. The unbinding force was calculated as the mean of the force values spanning that same region. This data was used to create the plots shown in Figure 4A-E. The unbinding forces were fit to a Gaussian mixture model (GMM) using an expectation maximization algorithm to determine the bins; the means and standard deviations used in the GMM fit were initialized using the k-means clustering algorithm. We determined the characteristic lifetime of each bin using maximum likelihood estimation (MLE) on

bootstrapped samples. The likelihood function, $\mathcal{L}(\theta; X) = \prod_{i=1}^{N} f_i(x_i; \theta)$, was formulated using an exponential distribution f.

Where, $f(x; \lambda) = \begin{cases} \lambda e^{-\lambda x} & x \geq 0, \\ 0 & x < 0. \end{cases}$

The MLE lifetimes were fit by Chi-squared minimization to one of two models: a composite slip-catch bond model or a catch bond model [39]. Assuming the errors in the measurements are Gaussian distributed, fitting by minimizing Chi-squared is the same as maximizing the log likelihood [39]. The composite slip-catch model used to fit the parental cell data was the sum of a slip bond model and a catch bond model. The slip bond model [38], $\tau(F) = \frac{1}{k_{off}(F)} = \tau(0)e^{-\frac{Fx_\beta}{k_B T}}$, was used as the first component of the composite slip-catch model to fit the parental cell data (Figure 4A), where τ is the characteristic bond lifetime in the absence of force and x_β is the reaction coordinate distance. The catch bond model used in the composite model and to fit all other cell lines is given by,

$$\tau(F) = \frac{\sqrt{\pi} r_0 (E_1 - 2F(d + r_0)) e^{\beta(E_0 + dF)} (e^{\beta F r_0} - 1)}{4D(\beta E_0)^{\frac{3}{2}} F \left(1 + \frac{r_0}{d}\right)^2 (1 - e^{\beta(2F(d + r_0) - E_1)})}$$

where r_0 is the natural bond length, d is the reaction coordinate (same as x_β for the slip bond model), E_0 and E_1 are components of the bond energy, $\beta = \frac{1}{k_B T}$ (k_B is the Boltzmann constant), and D is a diffusion constant ($D = \frac{k_B T}{6\pi\eta r_0}$). The number of bins used was established by fitting the force and lifetime data to the GMM using 5, 6, 7, or 8 bins (only 7 and 8 for parental cell data) for each cell line. The composite slip-catch and catch bond model fitted parameters are shown in Table S2. The Chi-squared fitting function was

acquired from the Mathworks File Exchange website (Generalized Nonlinear Non-analytic Chi-Square Fitting by Nathaniel Brahms, May 26, 2006).

The fraction of strand-swap and X-dimers calculated from Figure 4A were determined by integrating each component of the composite model (slip/catch models) in 5 pN bins from 5 to 150 pN to determine the slip/catch area of that bin. The number of data points in each bin that corresponded to the slip bond model, for example, was determined by,

$$\Delta n_{slip} = \left(\frac{\Delta A_{slip}}{\Delta A_{slip} + \Delta A_{catch}}\right)\Delta n$$

where ΔA_{slip} and ΔA_{catch} are the area under slip and catch bond fit respectively for the 5pN bin, and Δn is the total number of data points in the 5pN bin. As expected, the sum of the slip and catch bond fits—and therefore the sum of their areas—is equal to the composite fit. The total fraction of data corresponding to the slip bond (strand-swap dimers) is then,

$$Fraction_{slip} = \frac{\sum \Delta n_{slip}}{\sum \Delta n}$$

Acknowledgments

Research in the SS lab was supported in part by the National Science Foundation (PHY-1607550) and National Institute of General Medical Sciences of the National Institutes of Health (R01GM121885). Research in the SY lab was supported by NIH R03 EB021636, NSF 1562095 (SY, REU supplement to JC), and UC Davis Provost's Undergraduate

Fellowship (to JC). JC is a recipient of the Beckman Scholars Award. Research in the MG lab was supported by the Netherlands Organization for Scientific Research (NWO; 016.Vidi.189.166 and NWO gravitational program CancerGenomiCs.nl).

References

1. Mendonsa AM, Na T-Y, Gumbiner BM. E-cadherin in contact inhibition and cancer. *Oncogene* 2018, **37**(35)**:** 4769-4780.

2. Boggon TJ, Murray J, Chappuis-Flament S, Wong E, Gumbiner BM, Shapiro L. C-cadherin ectodomain structure and implications for cell adhesion mechanisms. *Science* 2002, **296**(5571)**:** 1308-1313.

3. Parisini E, Higgins JMG, Liu JH, Brenner MB, Wang JH. The crystal structure of human E-cadherin domains 1 and 2, and comparison with other cadherins in the context of adhesion mechanism. *J Mol Biol* 2007, **373:** 401-411.

4. Haussinger D, Ahrens T, Aberle T, Engel J, Stetefeld J, Grzesiek S. Proteolytic E-cadherin activation followed by solution NMR and X-ray crystallography. *EMBO J* 2004, **23**(8)**:** 1699-1708.

5. Sivasankar S, Zhang Y, Nelson WJ, Chu S. Characterizing the initial encounter complex in cadherin adhesion. *Structure* 2009, **17**(8)**:** 1075-1081.

6. Harrison OJ, Bahna F, Katsamba PS, Jin XS, Brasch J, Vendome J*, et al.* Two-step adhesive binding by classical cadherins. *Nat Struct Mol Biol* 2010, **17**(3)**:** 348-U121.

7. Hong SJ, Troyanovsky RB, Troyanovsky SM. Cadherin exits the junction by switching its adhesive bond. *J Cell Biol* 2011, **192**(6)**:** 1073-1083.

8. Rakshit S, Zhang Y, Manibog K, Shafraz O, Sivasankar S. Ideal, catch, and slip bonds in cadherin adhesion. *Proc Natl Acad Sci U S A* 2012, **109**(46)**:** 18815-18820.

9. Manibog K, Sankar K, Kim S-A, Zhang Y, Jernigan RL, Sivasankar S. Molecular determinants of cadherin ideal bond formation: Conformation-dependent unbinding on a multidimensional landscape. *Proc Natl Acad Sci U S A* 2016, **13**(139)**:** E5711-E5720

10. Manibog K, Li H, Rakshit S, Sivasankar S. Resolving the molecular mechanism of cadherin catch bond formation. *Nat Commun* 2014, **5:** 3941.

11. Ratheesh A, Yap AS. A bigger picture: classical cadherins and the dynamic actin cytoskeleton. *Nat Rev Mol Cell Biol* 2012, **13**(10)**:** 673-679.

12. Yonemura S, Wada Y, Watanabe T, Nagafuchi A, Shibata M. alpha-Catenin as a tension transducer that induces adherens junction development. *Nat Cell Biol* 2010, **12**(6)**:** 533-U535.

13. Kim T-J, Zheng S, Sun J, Muhamed I, Wu J, Lei L*, et al.* Dynamic visualization of α-catenin reveals rapid, reversible conformation switching between tension states. *Curr Biol* 2015, **25**(2)**:** 218-224.

14. Buckley CD, Tan J, Anderson KL, Hanein D, Volkmann N, Weis WI*, et al.* The minimal cadherin-catenin complex binds to actin filaments under force. *Science* 2014, **346**(6209)**:** 1254211.

15. Choi H-J, Pokutta S, Cadwell GW, Bobkov AA, Bankston LA, Liddington RC*, et al.* αE-catenin is an autoinhibited molecule that coactivates vinculin. *Proc Natl Acad Sci U S A* 2012, **109**(22)**:** 8576-8581.

16. Yao M, Qiu W, Liu R, Efremov AK, Cong P, Seddiki R*, et al.* Force-dependent conformational switch of α-catenin controls vinculin binding. *Nat Commun* 2014, **5**(4525).

17. le Duc Q, Shi Q, Blonk I, Sonnenberg A, Wang N, Leckband D*, et al.* Vinculin potentiates E-cadherin mechanosensing and is recruited to actin-anchored sites within adherens junctions in a myosin II-dependent manner. *J Cell Biol* 2010, **189**(7)**:** 1107-1115.

18. Seddiki R, Narayana GHNS, Strale P-O, Balcioglu HE, Peyret G, Yao M*, et al.* Force-dependent binding of vinculin to α-catenin regulates cell–cell contact stability and collective cell behavior. *Mol Biol Cell* 2018, **29**(4)**:** 380-388.

19. Barry AK, Tabdili H, Muhamed I, Wu J, Shashikanth N, Gomez GA*, et al.* α-catenin cytomechanics–role in cadherin-dependent adhesion and mechanotransduction. *J Cell Sci* 2014, **127**(8)**:** 1779-1791.

20. Thomas WA, Boscher C, Chu Y-S, Cuvelier D, Martinez-Rico C, Seddiki R*, et al.* α-Catenin and vinculin cooperate to promote high E-cadherin-based adhesion strength. *J Biol Chem* 2013, **288**(7)**:** 4957-4969.

21. Huveneers S, de Rooij J. Mechanosensitive systems at the cadherin-F-actin interface. *J Cell Sci* 2013, **126**(2)**:** 403-413.

22. Leckband D, de Rooij J. Cadherin adhesion and mechanotransduction. *Annu Rev Cell Dev Biol* 2014, **30:** 291-315.

23. Mège RM, Ishiyama N. Integration of cadherin adhesion and cytoskeleton at adherens junctions. *Cold Spring Harbor Perspect Biol* 2017, **9**(5)**:** a028738.

24. Ortega FE, Rengarajan M, Chavez N, Radhakrishnan P, Gloerich M, Bianchini J*, et al.* Adhesion to the host cell surface is sufficient to mediate Listeria monocytogenes entry into epithelial cells. *Mol Biol Cell* 2017**:** E16-12-0851.

25. Twiss F, Le Duc Q, Van Der Horst S, Tabdili H, Van Der Krogt G, Wang N*, et al.* Vinculin-dependent Cadherin mechanosensing regulates efficient epithelial barrier formation. *Biology open* 2012, **1**(11)**:** 1128-1140.

26. Hochmuth R, Evans E. Extensional flow of erythrocyte membrane from cell body to elastic tether. I. Analysis. *Biophys J* 1982, **39**(1)**:** 71-81.

27. Hochmuth R, Wiles H, Evans E, McCown J. Extensional flow of erythrocyte membrane from cell body to elastic tether. II. Experiment. *Biophys J* 1982, **39**(1)**:** 83-89.

28. Evans E, Heinrich V, Leung A, Kinoshita K. Nano-to microscale dynamics of P-selectin detachment from leukocyte interfaces. I. Membrane separation from the cytoskeleton. *Biophys J* 2005, **88**(3)**:** 2288-2298.

29. Sariisik E, Popov C, Müller JP, Docheva D, Clausen-Schaumann H, Benoit M. Decoding cytoskeleton-anchored and non-anchored receptors from single-cell adhesion force data. *Biophys J* 2015, **109**(7)**:** 1330-1333.

30. Schmitz J, Benoit M, Gottschalk K-E. The viscoelasticity of membrane tethers and its importance for cell adhesion. *Biophys J* 2008, **95**(3)**:** 1448-1459.

31. Heinrich V, Leung A, Evans E. Nano-to microscale dynamics of P-selectin detachment from leukocyte interfaces. II. Tether flow terminated by P-selectin dissociation from PSGL-1. *Biophys J* 2005, **88**(3)**:** 2299-2308.

32. Rimm DL, Koslov ER, Kebriaei P, Cianci CD, Morrow JS. Alpha 1 (E)-catenin is an actin-binding and-bundling protein mediating the attachment of F-actin to the

membrane adhesion complex. *Proc Natl Acad Sci U S A* 1995, **92**(19)**:** 8813-8817.

33. Desai R, Sarpal R, Ishiyama N, Pellikka M, Ikura M, Tepass U. Monomeric [alpha]-catenin links cadherin to the actin cytoskeleton. *Nat Cell Biol* 2013, **15**(3)**:** 261-273.

34. Huveneers S, Oldenburg J, Spanjaard E, van der Krogt G, Grigoriev I, Akhmanova A*, et al.* Vinculin associates with endothelial VE-cadherin junctions to control force-dependent remodeling. *J Cell Biol* 2012, **196**(5)**:** 641-652.

35. Sako Y, Nagafuchi A, Tsukita S, Takeichi M, Kusumi A. Cytoplasmic regulation of the movement of E-cadherin on the free cell surface as studied by optical tweezers and single particle tracking: corralling and tethering by the membrane skeleton. *J Cell Biol* 1998, **140**(5)**:** 1227-1240.

36. Krieg M, Helenius J, Heisenberg CP, Muller DJ. A bond for a lifetime: employing membrane nanotubes from living cells to determine receptor–ligand kinetics. *Angew Chem Int Ed* 2008, **47**(50)**:** 9775-9777.

37. Hosu BG, Sun M, Marga F, Grandbois M, Forgacs G. Eukaryotic membrane tethers revisited using magnetic tweezers. *Phys Biol* 2007, **4**(2)**:** 67.

38. Bell GI. Models for specific adhesion of cells to cells. *Science* 1978, **200**(4342)**:** 618-627.

39. Chakrabarti S, Hinczewski M, Thirumalai D. Plasticity of hydrogen bond networks regulates mechanochemistry of cell adhesion complexes. *Proc Natl Acad Sci U S A* 2014, **111**(25)**:** 9048-9053.

40. Evans E, Ritchie K. Dynamic strength of molecular adhesion bonds. *Biophys J* 1997, **72**(4)**:** 1541-1555.

41. Panorchan P, Thompson MS, Davis KJ, Tseng Y, Konstantopoulos K, Wirtz D. Single-molecule analysis of cadherin-mediated cell-cell adhesion. *J Cell Sci* 2006, **119**(1)**:** 66-74.

42. Shi QM, Maruthamuthu V, Li F, Leckband D. Allosteric Cross Talk between Cadherin Extracellular Domains. *Biophys J* 2010, **99**(1)**:** 95-104.

43. Shashikanth N, Petrova YI, Park S, Chekan J, Maiden S, Spano M*, et al.* Allosteric regulation of E-cadherin adhesion. *J Biol Chem* 2015, **290**(35)**:** 21749-21761.

44. Shashikanth N, Kisting MA, Leckband DE. Kinetic measurements reveal enhanced protein-protein interactions at intercellular junctions. *Sci Rep* 2016, **6:** 23623.

45. Kim M, Carman CV, Springer TA. Bidirectional transmembrane signaling by cytoplasmic domain separation in integrins. *Science* 2003, **301**(5640)**:** 1720-1725.

46. Bajpai S, Correia J, Feng YF, Figueiredo J, Sun SX, Longmore GD*, et al.* alpha-Catenin mediates initial E-cadherin-dependent cell-cell recognition and subsequent bond strengthening. *Proc Natl Acad Sci U S A* 2008, **105**(47)**:** 18331-18336.

47. Bajpai S, Feng Y, Krishnamurthy R, Longmore GD, Wirtz D. Loss of α-catenin decreases the strength of single E-cadherin bonds between human cancer cells. *J Biol Chem* 2009, **284**(27)**:** 18252-18259.

48. Nagafuchi A, Ishihara S, Tsukita S. The roles of catenins in the cadherin-mediated cell adhesion: functional analysis of E-cadherin-alpha catenin fusion molecules. *J Cell Biol* 1994, **127**(1)**:** 235-245.

49. Indra I, Choi J, Chen C-S, Troyanovsky RB, Shapiro L, Honig B*, et al.* Spatial and temporal organization of cadherin in punctate adherens junctions. *Proc Natl Acad Sci U S A* 2018, **115**(19)**:** E4406-E4415.

50. Wu Y, Kanchanawong P, Zaidel-Bar R. Actin-delimited adhesion-independent clustering of E-cadherin forms the nanoscale building blocks of adherens junctions. *Dev Cell* 2015, **32**(2)**:** 139-154.

51. Petrova YI, Spano MM, Gumbiner BM. Conformational epitopes at cadherin calcium-binding sites and p120-catenin phosphorylation regulate cell adhesion. *Mol Biol Cell* 2012, **23**(11)**:** 2092-2108.

52. Maiden SL, Petrova YI, Gumbiner BM. Microtubules inhibit E-cadherin adhesive activity by maintaining phosphorylated p120-catenin in a colon carcinoma cell model. *PLoS One* 2016, **11**(2)**:** e0148574.

53. Petrova YI, Schecterson L, Gumbiner BM. Roles for E-cadherin cell surface regulation in cancer. *Mol Biol Cell* 2016, **27**(21)**:** 3233-3244.

54. Li T, Guo H, Song Y, Zhao X, Shi Y, Lu Y*, et al.* Loss of vinculin and membrane-bound β-catenin promotes metastasis and predicts poor prognosis in colorectal cancer. *Mol Cancer* 2014, **13**(1)**:** 263.

55. Rodriguez Fernandez J, Geiger B, Salomon D, Sabanay I, Zöller M, Ben-Ze'ev A. Suppression of tumorigenicity in transformed cells after transfection with vinculin cDNA. *J Cell Biol* 1992, **119**(2)**:** 427-438.

56. Zhang Y, Sivasankar S, Nelson WJ, Chu S. Resolving cadherin interactions and binding cooperativity at the single molecule level. *Proc Natl Acad Sci U S A* 2009, **106**(1)**:** 109-114.

57. Longo PA, Kavran JM, Kim M-S, Leahy DJ. Transient mammalian cell transfection with polyethylenimine (PEI). *Methods in enzymology*, vol. 529. Elsevier, 2013, pp 227-240.

58. Shafraz O, Rübsam M, Stahley SN, Caldara AL, Kowalczyk AP, Niessen CM*, et al.* E-cadherin binds to desmoglein to facilitate desmosome assembly. *eLife* 2018, **7:** e37629.

59. Hutter JL, Bechhoefer J. Calibration of atomic-force microscope tips. *Rev Sci Instrum* 1993, **64**(7)**:** 1868-1873.

60. Yen C-F, Sivasankar S. Improving estimation of kinetic parameters in dynamic force spectroscopy using cluster analysis. *J Chem Phys* 2018, **148**(12)**:** 123301.

Figures

Figure 1. Overview of experiment. (A) The extracellular region of Ecad from opposing cells mediate adhesion. The cytoplasmic region of Ecad associates either directly or indirectly with p120 catenin, β-catenin, α-catenin, vinculin, and F-actin. **(B)** Biotinylated Ecad monomers were immobilized on an AFM cantilever functionalized with Polyethylene glycol (PEG) and Streptavidin as described in the methods section. Interactions between Ecads on the cantilever and Ecads expressed on the apical surface of MDCK cells were

measured. **(C)** Western blot analysis of cell lysates of the parental and engineered MDCK cell lines used in experiments.

Figure 2. Role of α-catenin and vinculin in Ecad-cytoskeleton linkage. (A) Binding probabilities were measured using AFM cantilevers lacking Ecad (control experiment, light gray) or AFM cantilevers decorated with Ecad (Ecad, dark blue). Total number of Ecad/control measurements performed on each cell line were 6793/3361 measurements on parental cells, 7268/4858 measurements on parental-Trp, 4291/3666 measurements on vinc-KO cells, 4518/3381 measurements on αcat-KO cells, 6124/6070 measurements on ΔVBS cells, and 3672/2449 measurements on Ecad-KO cells. Error bars are bootstrapped standard deviations. **(B)** Fraction of uncoupled (membrane-tether) and coupled (cyto-tether + jump) events. Fractions were calculated after subtracting the binding probability of the control experiment for each cell line. Error bars are the propagated errors obtained from bootstrapped standard deviations.

Figure 3. Force 'signatures' used to identify cytoskeletal coupling and strength of *trans* adhesion. (A) Typical force curve showing a membrane-tether which extends at a constant force. **(B)** Membrane tethers are measured when an Ecad, which is not linked to the actin cytoskeleton is pulled. **(C)** Jump events exhibit a linear increase in force and are measured upon pulling **(D)** an Ecad *trans* dimer that is weaker than its cytoskeleton coupling. **(E)** Typical force curve showing a cyto-tether with an initial increase in force that

viscoelastically relaxes as a membrane-tether is formed. **(F)** Cyto-tethers are measured when a robust Ecad *trans* dimer that is linked to the actin cytoskeleton is pulled.

Figure 4. Measuring conformation of Ecad *trans* dimers using an AFM. Force *vs* lifetime profile for **(A)** parental cells show that 73% of Ecad form slip bonds while the remaining 27% form catch bonds. **(B)** parental-Trp, **(C)** vinc-KO, **(D)** αcat-KO, and **(E)** ΔVBS cells form catch bonds. Solid lines represent fits to the corresponding models. Data was binned using a Gaussian mixture model and the lifetimes were determined using maximum likelihood estimation. The data was fit by χ^2 minimization and errors were obtained by bootstrapping. The y-axis in (A-E) were limited to 1s for clarity. **(F)** Fractions of strong (cyto-tether) and weak (jump) Ecad *trans* dimer events. Error bars are the propagated errors obtained from bootstrapped standard deviations.

Figure 1

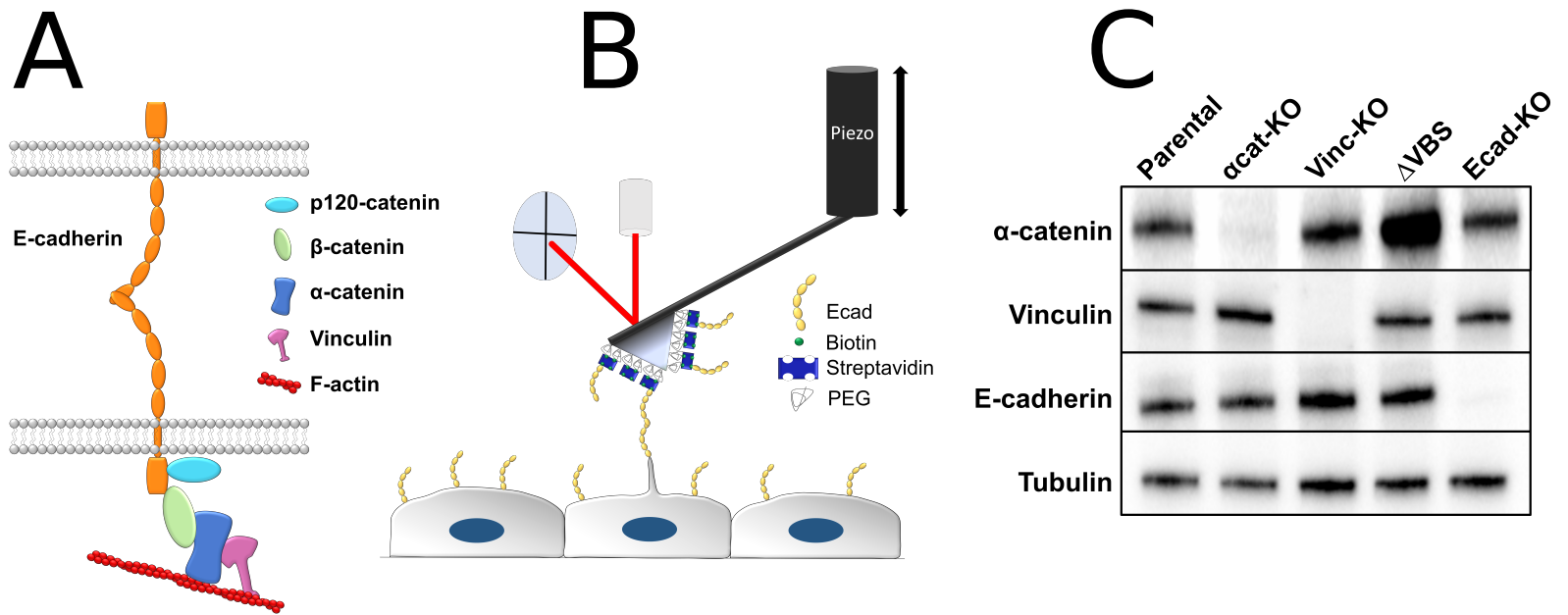
A
E-cadherin
p120-catenin
β-catenin
α-catenin
Vinculin
F-actin
B
Piezo
Ecad
Biotin
Streptavidin
PEG
C
Parental
αcat-KO
Vinc-KO
ΔVBS
Ecad-KO
α-catenin
Vinculin
E-cadherin
Tubulin

Figure 2

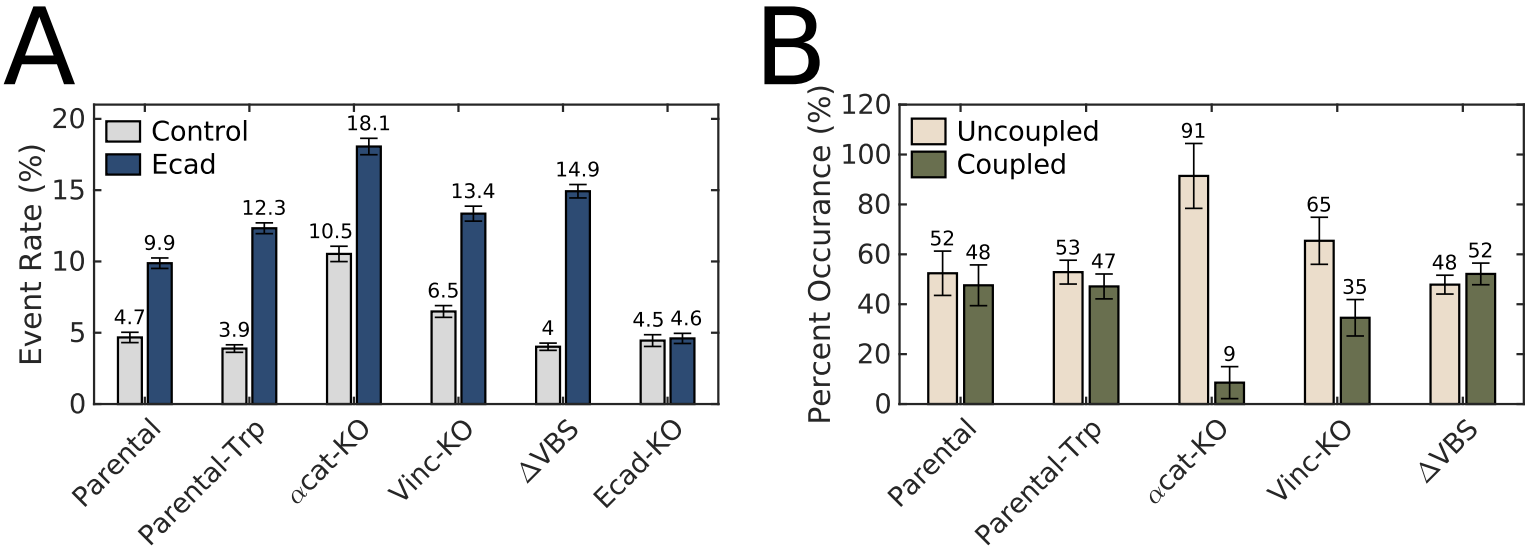
A
Control
Ecad
Event Rate (%)
0
5
10
15
20
4.7
9.9
3.9
12.3
10.5
18.1
6.5
13.4
4
14.9
4.5
4.6
Parental
Parental-Trp
αcat-KO
Vinc-KO
ΔVBS
Ecad-KO
B
Uncoupled
Coupled
Percent Occurance (%)
0
20
40
60
80
100
120
52
48
53
47
91
9
65
35
48
52
Parental
Parental-Trp
αcat-KO
Vinc-KO
ΔVBS

Figure 3

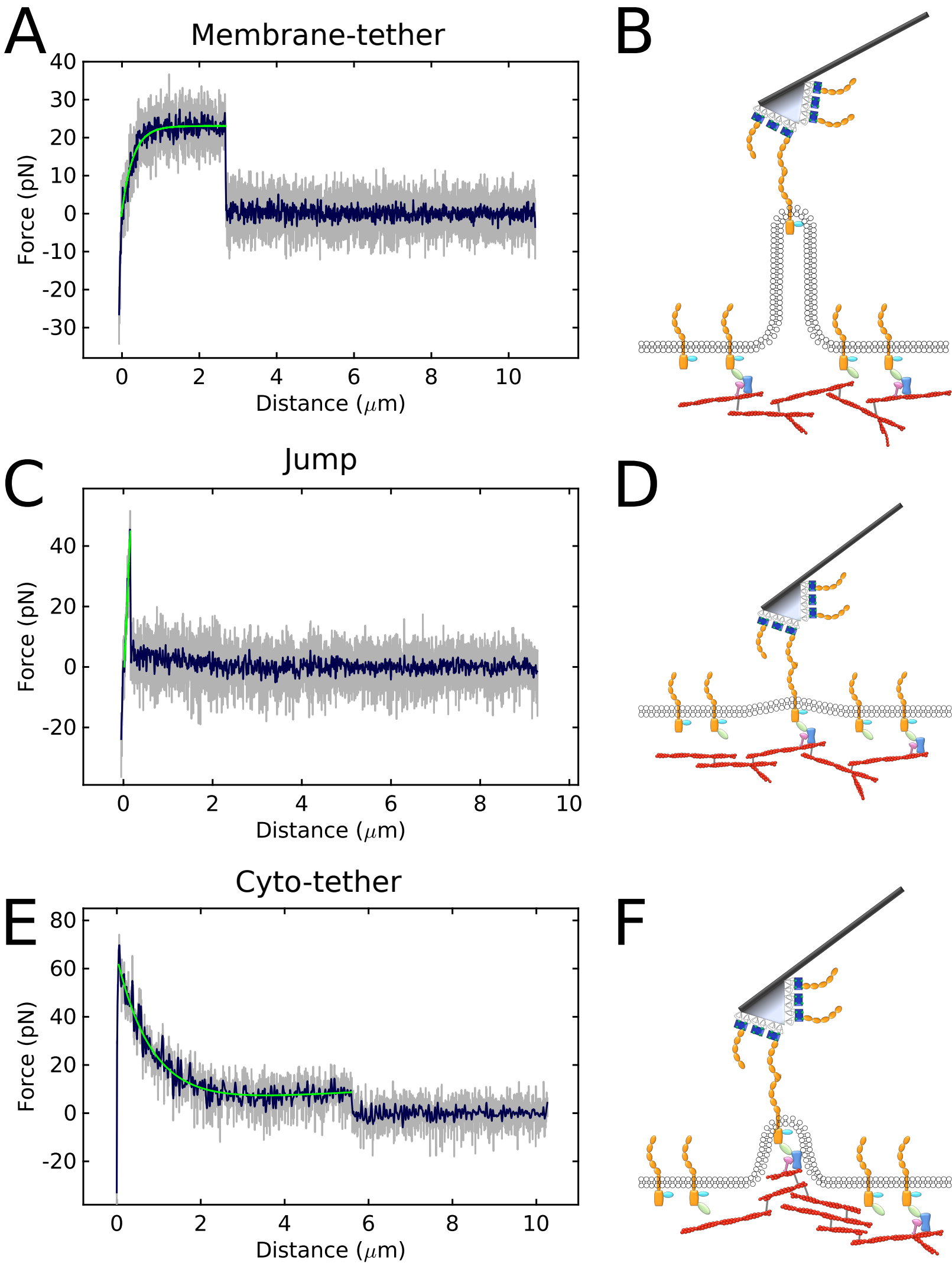
A
Membrane-tether
Force (pN)
Distance (μm)
B
C
Jump
Force (pN)
Distance (μm)
D
E
Cyto-tether
Force (pN)
Distance (μm)
F

Figure 4

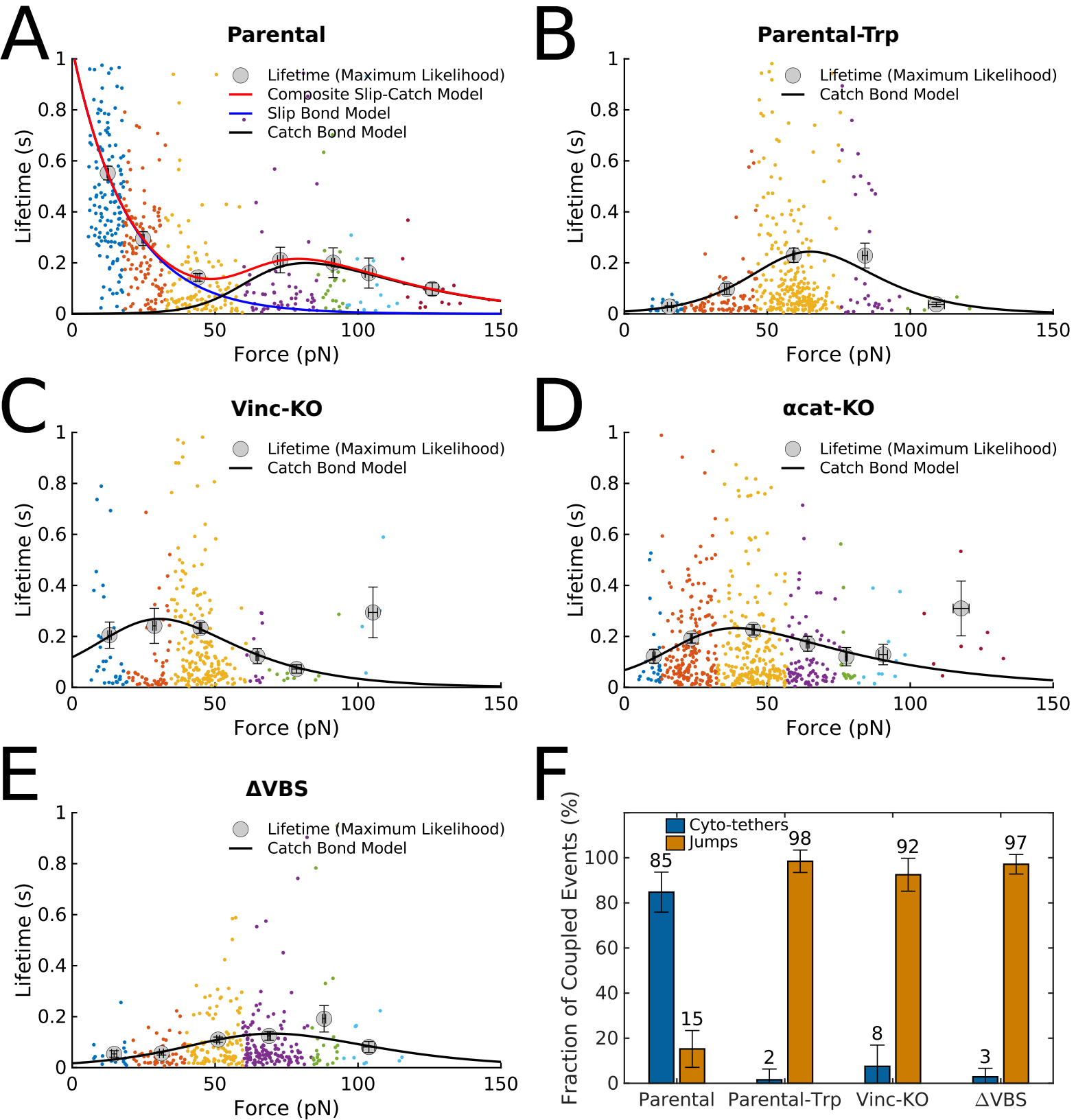
A
Parental
Lifetime (Maximum Likelihood)
Composite Slip-Catch Model
Slip Bond Model
Catch Bond Model
Lifetime (s)
Force (pN)
B
Parental-Trp
Lifetime (Maximum Likelihood)
Catch Bond Model
Lifetime (s)
Force (pN)
C
Vinc-KO
Lifetime (Maximum Likelihood)
Catch Bond Model
Lifetime (s)
Force (pN)
D
αcat-KO
Lifetime (Maximum Likelihood)
Catch Bond Model
Lifetime (s)
Force (pN)
E
ΔVBS
Lifetime (Maximum Likelihood)
Catch Bond Model
Lifetime (s)
Force (pN)
F
Cyto-tethers
Jumps
Fraction of Coupled Events (%)
85
15
2
98
8
92
3
97
Parental
Parental-Trp
Vinc-KO
ΔVBS